High-Height Long-Period Ocean Waves Generated by a Severe Storm in the Northeast Pacific Ocean during February 1983

MARSHALL D. EARLE AND KATHRYN A. BUSH[1]

Marine Environments Corporation, Manassas, VA 22110

GLENN D. HAMILTON

NOAA Data Buoy Center, NSTL Station, MS 39529

(Manuscript received 16 September 1983, in final form 1 June 1984)

ABSTRACT

Unusually severe storms occurred in the northeast Pacific Ocean between January and March 1983, and waves from these storms caused extensive erosion and damage along the U.S. west coast. Wave conditions as measured by eight data buoys are described for an intense storm off northern California with significant wave heights up to 12.9 m that occurred during February 1983. A very uncommon feature of the wave spectra is considerable energy at long periods of 20 to 25 s. Long period waves were generated west of the northern buoys and propagated as high swell to the southern buoys. Swell propagation was consistent with classical wave theory. The ability to quantitatively identify high swell at northern buoys prior to its arrival at buoys off southern California may have real-time swell forecast applications. Differences between measurements and numerical wave model forecasts and hindcasts indicate the value of the wave data and areas where numerical modeling of such storm-generated waves could be improved.

1. Introduction

Several severe storms moved across the northeast Pacific Ocean during January, February and March of 1983. Waves generated by these storms caused unusually extensive erosion and damage along the U.S. west coast, particularly the California coast. Wave conditions during these storms were measured by data buoys operated by the National Oceanic and Atmospheric Administration (NOAA) Data Buoy Center (NDBC). Wave spectra associated with one storm in February 1983 had considerable wave energy at unusually long periods of 20–25 s. Wave conditions were severe with a maximum significant wave height of 12.9 m at the buoy closest to the storm. For a Rayleigh distribution of wave heights and 1000 waves, this significant wave height corresponds to a probable maximum wave height of approximately 24 m.

Figure 1 shows the track of the center of this storm and the positions of the data buoys from which data were examined for this study. NDBC typically has 14 to 16 buoys with operating wave measurement capability deployed in the northeast Pacific Ocean region. Data from buoys at eight stations were primarily used for this study. Except at station 46025, located where the water depth is 183 m, water depths are deep enough for waves to be negligibly affected by the bottom. Waves reaching station 46025 are also partly blocked by offshore islands. The measured long period waves during high sea states are most unusual. Such long wave periods have seldom been measured during high sea states by NOAA data buoys which have been deployed with wave measurement capability at many locations since the mid-1970s (e.g., NOAA Data Buoy Center, 1983). The eight stations primarily used for this study were spread along the U.S. west coast with one station near the region of most active wave generation. The stations thus serve as a network for examination of wave characteristics associated with severe northeast Pacific Ocean storms and propagation of high swell to coastal locations. High swell is of major practical interest because swell from northeast Pacific Ocean storms is an important cause of erosion and damage along the California coast.

The purpose of this paper is to document and describe both the meteorological situation causing the unusual wave conditions and the wave conditions themselves. The wave measurements are unique for three main reasons. First, they were made by many independently operating buoys at different locations thus providing confidence in the measurements and a description of how wave conditions vary with location. Second, the very long periods are rare and may not be well accounted for by wave formulations

[1] Present affiliation: Skidaway Institute of Oceanography.

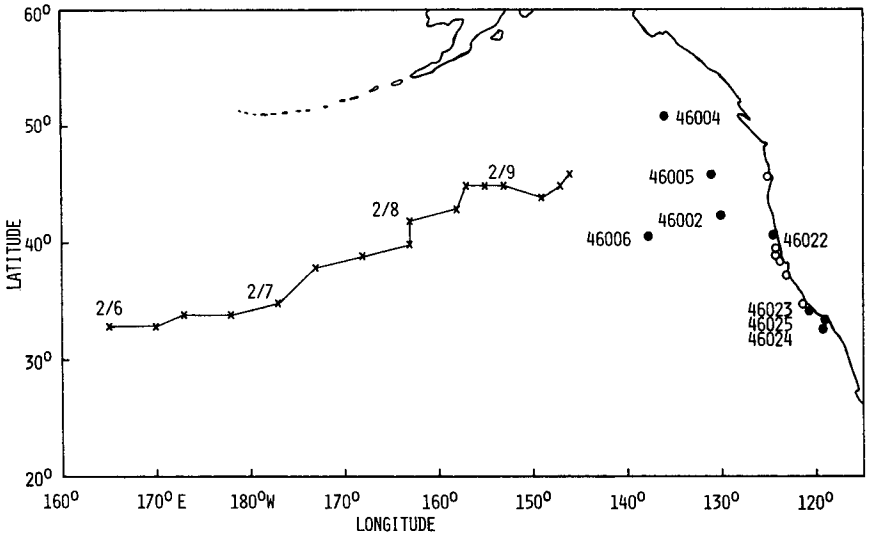

FIG. 1. Storm track and locations of data buoys. Locations emphasized for this paper are indicated by buoy station numbers.

that are commonly used in numerical wave models. Third, the documented storm is an excellent example of the type of storm which causes serious problems along the west coast and the paper describes how measurements such as these would be useful to improve wave forecasts, especially for the southern California coast. For example, long period storm generated swell was measured at the northern buoys approximately 24 to 36 h before its arrival at the southern buoys.

2. Meteorological situation

The meteorological situation causing the high wave height and long wave period event was determined from Northern Hemisphere surface weather charts prepared by the NOAA National Meteorological Center (NMC), ship observations transmitted to NMC, and satellite images from the GOES-West satellite operated by NOAA. The regular GOES (Geostationary Operational Environmental Satellite) satellite had ceased operating the previous fall and the standby satellite provided only visual images rather than infrared images thus limiting satellite images to daylight hours. Figure 1 illustrates the storm track, as represented by the position of the center of lowest surface atmospheric pressure, relative to the data buoy locations. This particular storm was one of a series of storms between January and March that itensified in the northeast Pacific Ocean and which generated high wave conditions along and off the west coast of the United States.

The storm developed as an extratropical cyclone with wind circulation about a well-defined low pressure center on 6 February 1983. Figure 2 is the synoptic weather chart showing the storm at 1200 GMT on this day. The storm's central pressure at the surface was 992 mb and ship reported wind speeds were 10–12 m s^{-1}. The storm deepened rapidly and

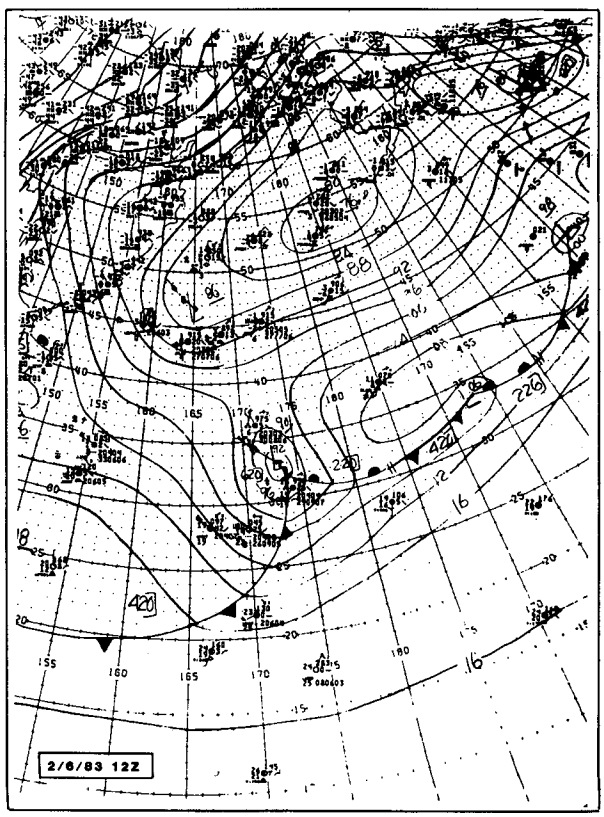

FIG. 2. Surface synoptic weather chart for 1200 GMT 6 February. Data buoy locations are indicated by triangles in this and the following weather charts.

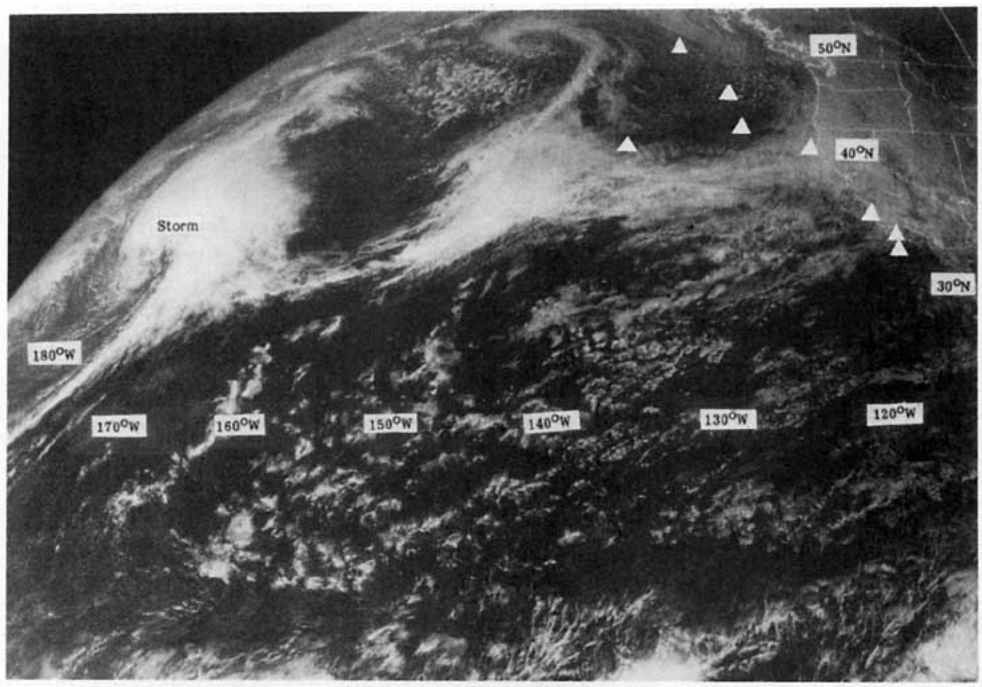

FIG. 3. GOES visual image at 2345 GMT 6 February. Data buoy locations are indicated by triangles in this and the following GOES visual images.

by 0000 GMT 7 February, the central pressure had fallen to 968 mb with ship reported wind speeds between 25 and 30 m s^{-1}. Near this time, the storm is clearly evident in the visual satellite image shown in Fig. 3. Fig. 4 is the synoptic weather chart for 1200 GMT 7 February. Fetch distances over which wind directions were relatively constant southeast of the storm center were on the order of 1000 km indicating generation of high waves. The storm continued to increase in intensity reaching its greatest wave generation potential, in terms of wind speeds and large fetch regions, between 0000 GMT and 1800 GMT 8 February. By 0000 GMT surface pressure at the storm center was 952 mb and winds measured by ships were sometimes above 30 m s^{-1}. Near this time, the storm is the dominant meteorological feature in the northeast Pacific Ocean as shown in the visual satellite image in Fig. 5. The synoptic weather chart for 1200 GMT 8 February is shown in Fig. 6. Wave generation regions south of the storm center had fetches between approximately 1000 km and 1500 km with approximately parallel isobars indicating waves propagating eastward toward the west coast. The surface central pressure was 952 mb, and ship reported wind speeds in wave generation regions south of the storm center ranged up to approximately 30 m s^{-1}. This chart also shows a second storm to the southwest with a central pressure of 980 mb. This second storm had formed about twelve hours earlier and later became another major

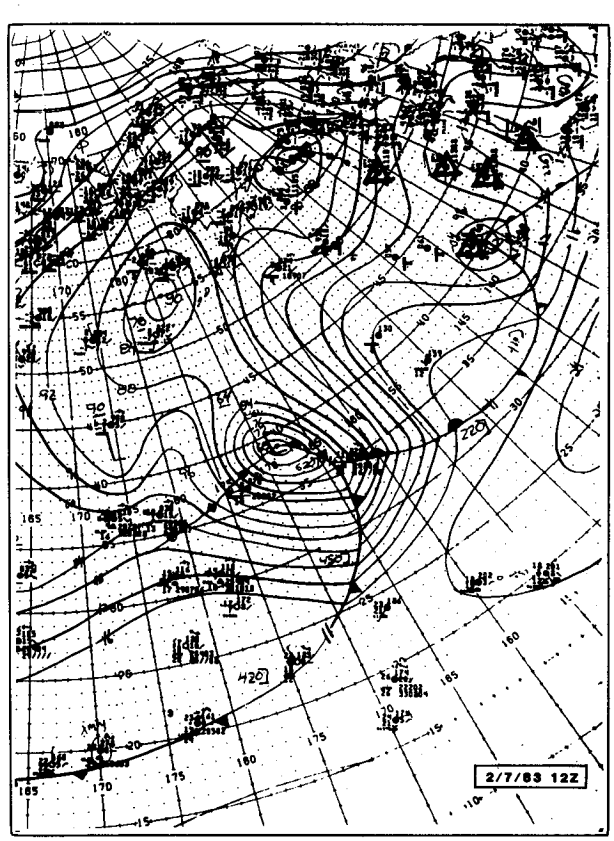

FIG. 4. As in Fig. 2 but for 1200 GMT 7 February.

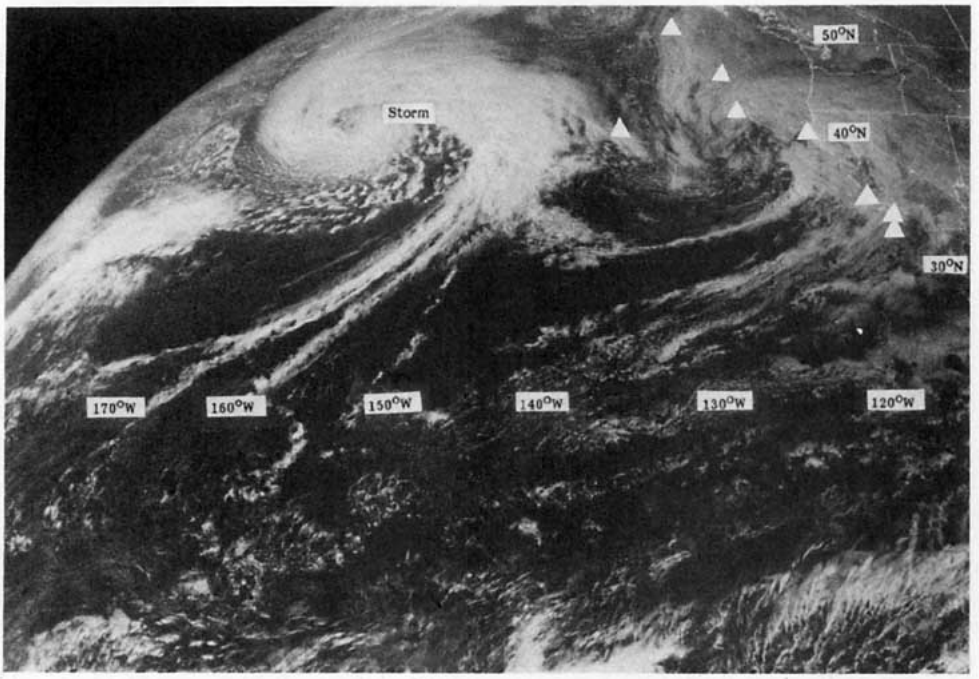

FIG. 5. As in Fig. 3 but at 2345 GMT 7 February.

storm. This pair of storms partly illustrates the sequence of severe storms which battered the U.S. west coast during January through March 1983. Largest wave generation fetches of roughly 1500 km occurred near 1800 GMT 8 February as shown in Fig. 7 which also shows the developing second storm. Winds mainly between 25 and 30 m s^{-1} in regions south of the storm center generated high waves propagating eastward. By 0000 GMT 9 February the primary eastern storm had filled considerably with a central pressure of 972 mb as shown in Fig. 8. The longest wave generation fetches were still oriented eastward. Fig. 9 is the satellite image near this time and shows that the second storm is now becoming the most important

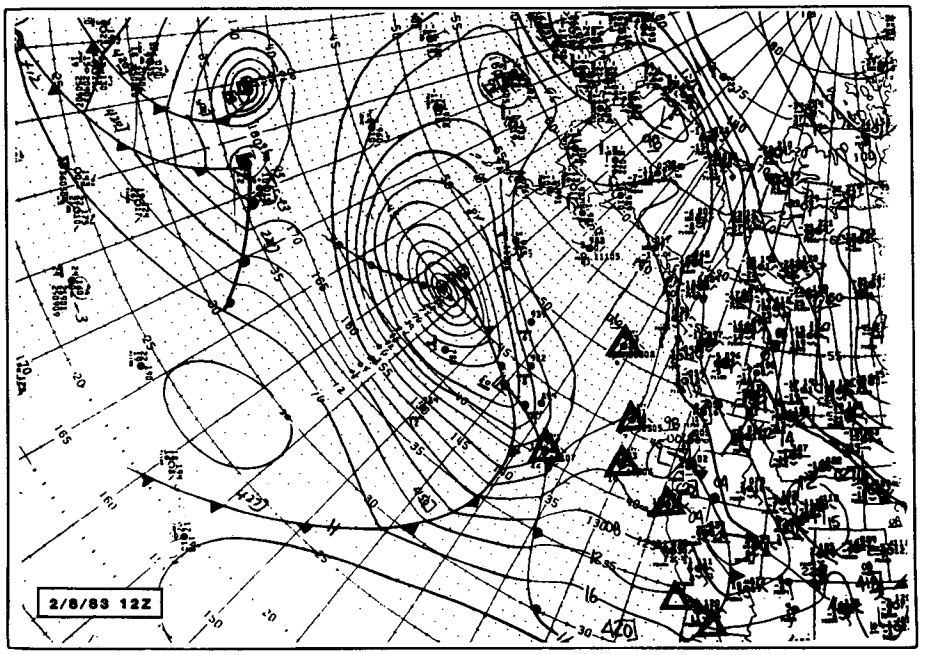

FIG. 6. As in Fig. 2 but for 1200 GMT 8 February.

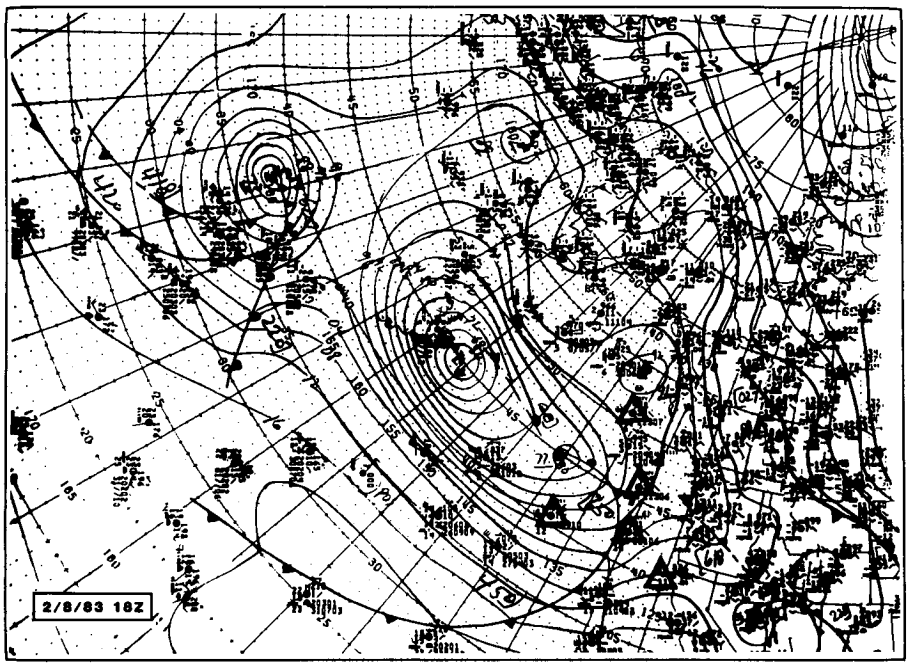

FIG. 7. As in Fig. 2 but for 1800 GMT 8 February.

storm. For the first storm, several ship visual wave observations, which are subjective and may have large uncertainties, indicated locally-generated sea-wave heights around 8 m and swell heights between 8 m and 10 m on 8 and 9 February. Ship observed swell periods ranged from 10 to 26 s. While the first storm continued to weaken, long wave generation fetches on the order of a 1000 km continued to exist as illustrated in Fig. 10 for 1200 GMT 9 February. After this time, the first storm became unimportant showing that its existence as a major storm covered an approximate three day time period. The second western

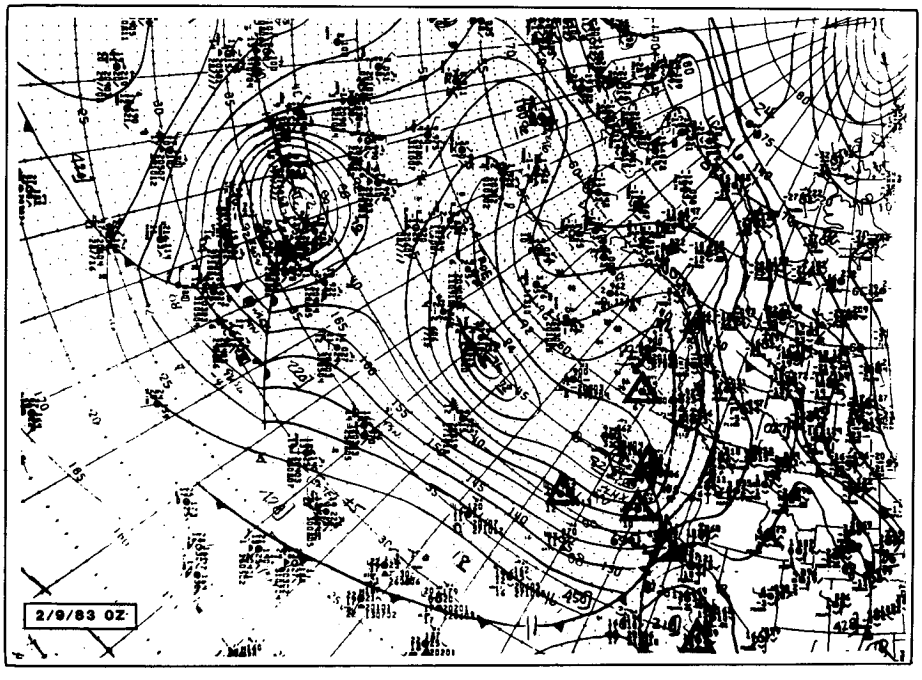

FIG. 8. As in Fig. 2 but for 0000 GMT 9 February.

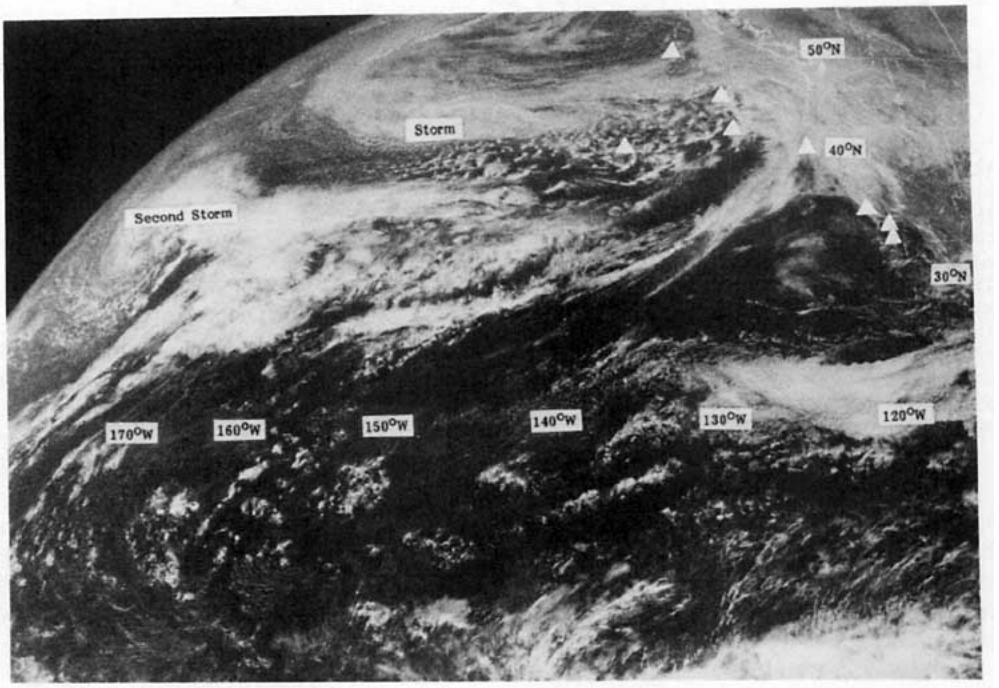

FIG. 9. As in Fig. 3 but at 2245 GMT 8 February.

storm had now become the major storm in the area. While the second storm is not of primary interest for this paper, it also produced high waves with long periods although the waves were not as high and the periods were not as long at most of the data buoys as those from the first storm.

3. Wave measurements

Wave data were used from the buoys in Table 1 which lists the station number, position, water depth and type of each buoy. Buoys are referenced by their World Meteorological Organization station numbers.

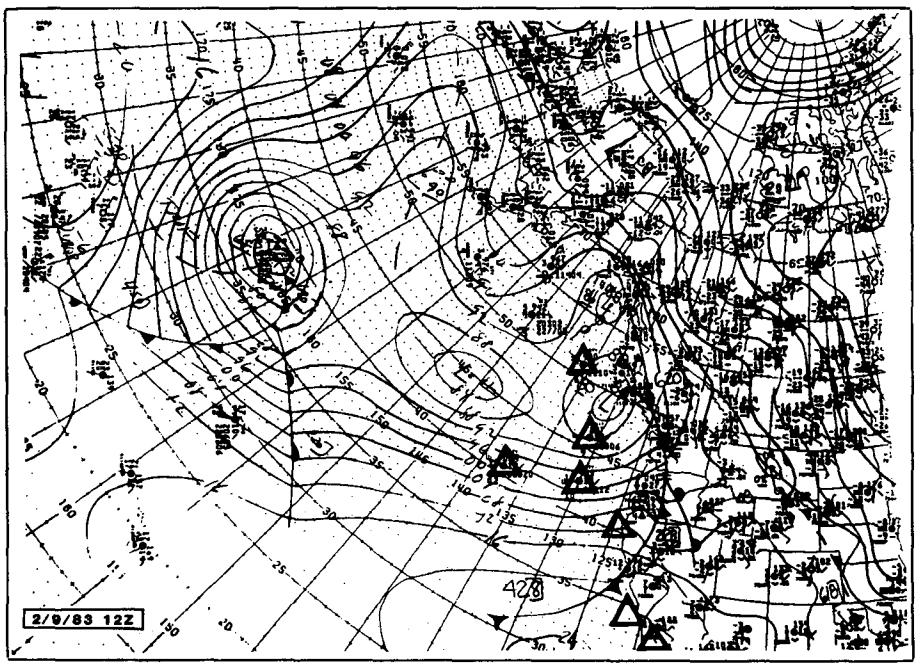

FIG. 10. As in Fig. 2 but for 1200 GMT 9 February.

TABLE 1. Data buoy information.

Station*	Latitude	Longitude	Water depth (m)	Buoy type
46002	42.50°N	130.00°W	3,384	6 m NOMAD
46004	51.00°N	136.00°W	3,567	12 m Discus
46005	46.00°N	131.00°W	2,851	12 m Discus
46006	40.70°N	137.70°W	3,963	12 m Discus
46022	40.80°N	124.50°W	311	10 m Discus
46023	34.30°N	120.70°W	622	6 m NOMAD
46024	33.00°N	119.20°W	823	10 m Discus
46025	33.80°W	119.30°W	183	6 m NOMAD

* These numbers are the World Meteorological Organization (WMO) station location numbers. At different times, different individual buoys may be at these locations.

Wave measurements were made with onboard instrumentation called Wave Data Analyzer (WDA) systems to distinguish these systems from other NDBC wave measurement systems. Details of the data collection and analysis procedures for WDA systems are described by Steele and Earle (1979). The basic wave sensor in these systems is a strapped-down accelerometer fixed in the buoy with its measurement axis perpendicular to the buoy deck. All sensors and electronic components on data buoys are tested by standard procedures and records for all sensors are maintained in NDBC files. Measured acceleration records are twenty minutes long with a sampling interval of 0.667 s. After appropriate signal conditioning such as use of anti-aliasing filters, accelerometer records are digitized and acceleration spectra are calculated by onboard microprocessors. Spectra are transmitted to shore hourly via GOES satellite. Acceleration spectra are corrected for low-frequency noise caused by strapping-down of the accelerometer, for filter responses during signal conditioning, and for buoy hull/mooring responses. Displacement spectra, which are standard wave spectra, are obtained from acceleration spectra by division of acceleration energy in each frequency band by radian center frequency to the fourth power. Wave spectra extend from 0.01 to 0.50 Hz in 0.01 Hz intervals although spectra are not normally used for frequencies less than 0.03 Hz where there is negligible wind-generated wave energy. Twenty-four degrees of freedom are associated with each spectral estimate.

Effects of strapped-down accelerometers were negligible for the data used in this study. NDBC operational data buoys, originally designed to monitor meteorological data, use strapped-down accelerometers for wave measurements because vertically-stabilized accelerometers (e.g., gryoscope type devices) are expensive, power consuming and unreliable for long operational deployments. As a result of buoy tilts in response to wave slopes, use of strapped-down accelerometers causes measured buoy vertical acceleration to be contaminated by buoy horizontal acceleration and a time-varying part of the acceleration due to gravity. Calculated acceleration spectra have small levels of excess low-frequency energy which are approximately corrected for during analysis. Previous computer simulations of accelerometer measurements (Earle and Bush, 1982) had documented errors due to use of strapped-down accelerometers for Pierson-Moskowitz spectra with cosine-squared directional spreading functions for significant wave heights up to 15 m, which is higher than the measured wave heights. These simulations used the same data analysis techniques as used for measured data. Based on the previous simulations and additional similar simulations, use of strapped-down accelerometers causes a maximum 3% over-estimate of significant wave height for the highest wave heights used in this study and cannot artificially shift measured spectra to incorrectly low frequencies. In addition, strapped-down accelerometer errors are much smaller than 90% statistical confidence intervals for both significant wave heights and spectra.

Figure 11 provides examples of time histories of spectral energy density in the low frequency bands centered at 0.04 and 0.05 Hz (periods of 25 and 20 s) at three stations. Station 46006 is closest to the storm, station 46022 is near the coast almost directly to the east of the storm, and station 46023 is off southern California. Initial arrival times and peaks of the longer period wave energy are before those of the shorter period wave energy. Initial arrival of swell from the second storm is seen on the righthand side of Fig. 11a. Fig. 12 shows corresponding time histories of significant wave height and dominant wave period. Significant wave height was computed from each spectrum by

$$H_S = 4\ (\text{Total Energy})^{1/2}, \qquad (1)$$

where the total energy was obtained by integration of the spectrum over all frequencies and equals the variance about the mean of the wave record. Because of finite spectral width effects, spectrally calculated significant wave heights are typically a few percent higher than significant heights obtained by averaging the highest one-third waves in a time series wave record (e.g., Longuet-Higgins, 1980). Dominant wave period was defined as the period corresponding to the center frequency of the frequency band with maximum spectral energy density. The dominant wave period plots are somewhat "jumpy" because of the 0.01 Hz resolution of the frequency bands. The high wave height and long period event associated with the storm is evident in the time histories of low-frequency wave energy, dominant wave period and significant wave height. Maximum wave energy in the low frequency bands, highest significant wave heights, and longest dominant wave periods occur

first at the northern stations closest to the storm track and later at the southern stations. Consistent behavior was seen in the wave data from all eight stations. Table 2 lists wave information at the time of the highest significant wave height at each station. Figure 13 shows examples of wave spectra near the times of highest significant wave heights at stations 46006, 46022, and 46023.

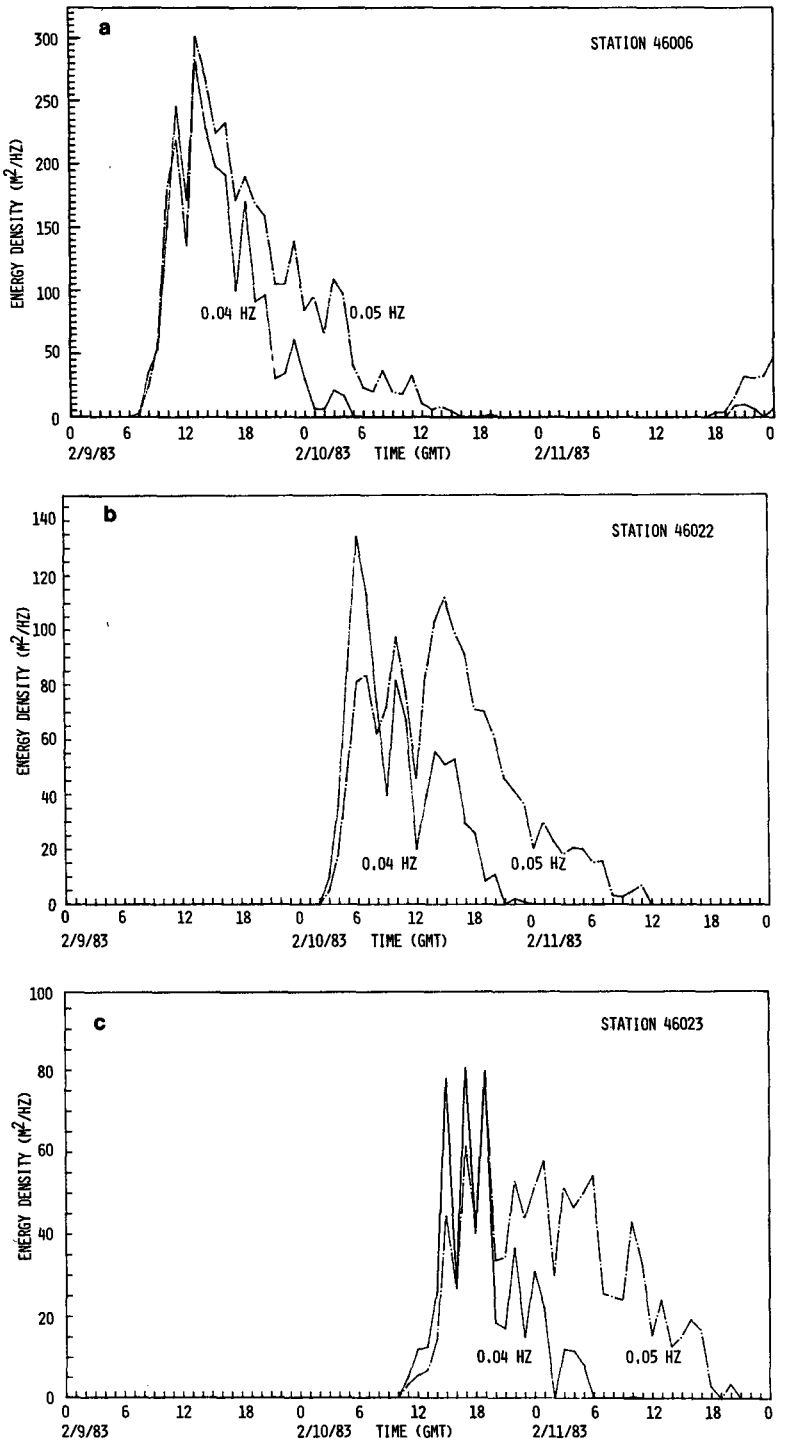

FIG. 11(a–c). Examples of time histories of low-frequency energy density at frequencies of 0.04 and 0.05 Hz.

4. Swell characteristics

The meteorological situation and the wave measurements show that high waves propagated from storm regions with high wind speeds and were not primarily generated near the data buoys. Near and at the times of highest significant wave heights, wave conditions tended to be swell-dominated. In other

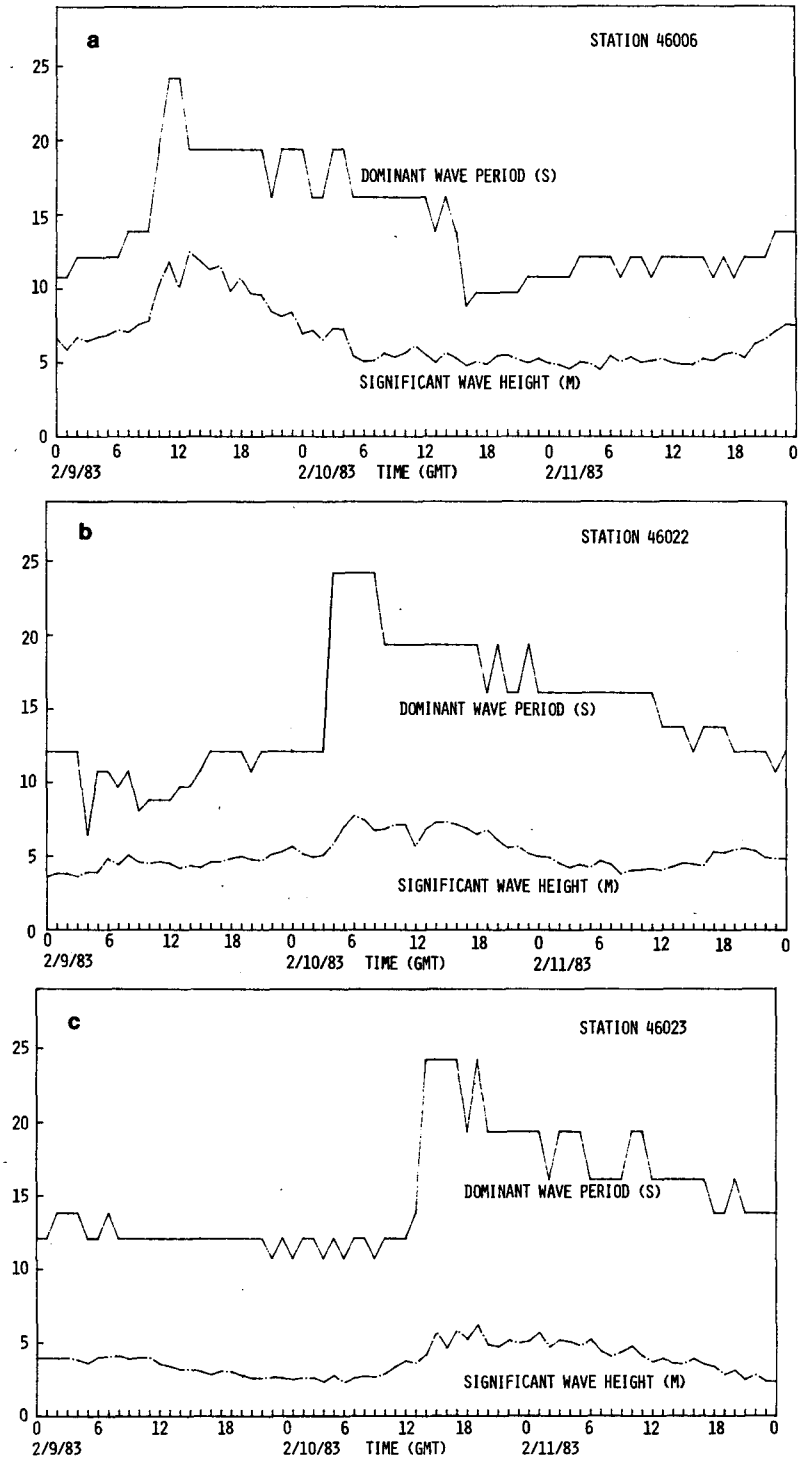

FIG. 12(a–c). Examples of time histories of dominant wave period and significant wave height.

TABLE 2. Buoy measurements at times of highest significant wave heights.

Station	Maximum H_S (m)	Dominant wave period (s)	Swell parameter (γ)	Wind speed (m s^{-1})	Anemometer elevation (m)	Time (GMT)/Date
46002	8.85	20.0*	19.1	4.0	5	0700 February 10
46004	6.57	16.7**	18.6	3.8	10	0500 February 10
46005	8.67	20.0*	31.0	3.4	10	0600 February 10
46006	12.85	20.0*	1.8	17.2	10	1300 February 9
46022	7.96	25.0	6.4	7.1	10	0600 February 10
46023	6.40	25.0	2.9	8.8	5	1900 February 10
46024	7.11	20.0*	10.1	5.4	10	0400 February 11
46025	2.71	16.7***	64.0	1.2	5	0900 February 11

* Dominant periods of 25.0 s occurred earlier.
** Dominant periods of 20.0 and 25.0 s occurred earlier.
*** A dominant period of 20.0 s occurred earlier.

words, wave heights were higher than those which would be generated by local winds. The relative importance of swell compared to locally-generated seas can be estimated from the ratio of measured significant wave height to the fully-developed significant wave height for the local wind speed. This ratio is given by

$$\gamma = \frac{H_S}{H_S\,(\text{Pierson-Moskowitz})} = 47.17\left(\frac{H_S}{u^2}\right), \quad (2)$$

where H_S is in meters and u is the wind speed in m s^{-1} at 19.5 m elevation. Table 2 lists values of γ at the times of highest significant wave heights for each station. The lowest value is at station 46006 which is nearest to the primary wave generation region. Local wind speeds were relatively high (approximately 9 m s^{-1}) at station 46023 causing a relatively small value. For station 46025, wind speeds were very low (~1–2 m s^{-1}) causing γ values to be sensitive to small wind speed changes. An average of wind speeds over a few hours, which is not important for these interpretations, would reduce wind variability effects. Table 2 shows the importance of swell as a major contributor to high wave conditions at the data buoys. There are other less direct methods, such as use of a parameter which is inversely proportional to wave steepness (e.g., Parsons, 1979) or use of wave age (e.g., Sverdrup and Munk, 1947) which provide indications of the importance of swell similar to interpretations of Table 2. Wave age is the ratio of wave phase speed to local wind speed.

High wave conditions along the west coast are frequently due to high swell from storm track regions of the northeast Pacific Ocean so that swell propagation is of interest. Wave energy travels along great circle routes at the frequency-dependent group velocity given by

$$v(f) = \frac{g}{4\pi f}, \quad (3)$$

where g is the acceleration due to gravity. Swell generated at time t_0 arrives at a location a distance d away at the time t_a given by

$$t_a = t_0 + \frac{d}{v(f)}. \quad (4)$$

Differentiation of Eq. (4) shows that the distance can be calculated from

$$\frac{dt_a}{df} = \frac{4\pi d}{g} \approx \left(\frac{t_2 - t_1}{f_2 - f_1}\right), \quad (5)$$

where t_1 and t_2 are arrival times of energy at frequencies f_1 and f_2 respectively. Because of the dispersive nature of swell propagation, the difference in arrival times of energy at different frequencies can be used to calculate propagation distances. Similarly, if the distance and arrival time is known, Eq. (4) can be used to obtain the generation time. Distances and generation times may also be estimated graphically

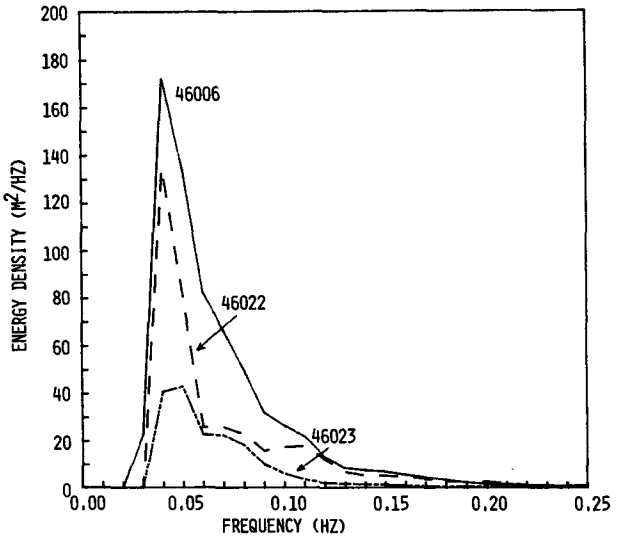

FIG. 13. Examples of wave spectra near times of highest significant wave heights.

using a frequency versus time plot of energy as described by Snodgrass *et al.* (1966). Analytical rather than graphical methods were used here.

Equations (4) and (5) with a single generation time and propagation distance strictly apply only if a storm is a point source in space and time. Otherwise, waves propagating to a location are a combination of waves generated at different places and times. Nevertheless, the classical concepts of swell propagation described by these equations provide swell propagation distances as shown in Table 3 which are consistent with the meteorological situation. Distances to each of the eight stations were calculated from the wave data using measured peak energy arrival times for the frequencies listed in parentheses in the table. The two lowest frequencies seen at each buoy were used to obtain peak energy arrival times. However, at stations 46004 and 46023 there was not a sufficient difference in peak energy arrival times at these frequencies for a distance calculation to be made. At these two buoys, peak energy arrival times at frequencies of 0.05 Hz and 0.06 Hz were used. The lowest frequency reaching station 46025 was 0.050 Hz, so peak energy arrival times at 0.05 Hz and 0.06 Hz were used. Station 46006, closest to the storm, was a special case since 0.03 Hz wave energy was briefly measured. Swell generation times were estimated from Eq. (4) using the calculated propagation distances with the group velocity associated with the lower of the two frequencies. Because of the storm size and its distance from the buoys, the storm is not truly a point source so that swell at each buoy would not propagate over a single distance. Locations representing the storm center and the face of the overall wave generation fetch toward the buoys were thus selected to bracket the main region of wave generation. These locations were obtained manually from the synoptic weather charts at the calculated generation times. Great circle distances between these storm locations and each buoy were calculated and are listed in Table 3. Since weather charts are only available at 6 h intervals, calculated distances were interpolated where necessary to obtain distances corresponding to the appropriate generation times. As seen in Table 3, distances estimated from the weather charts generally bracket the calculated distances from the measurements, indicating the consistency of the measurements with classical swell propagation theory. The wave generation times based on the measurements and swell propagation theory indicate that low-frequency wave energy left the storm region between 0000 GMT 8 February and 1200 GMT 9 February.

TABLE 3. Comparison of swell propagation distances from the storm to the buoys calculated from wave theory and from weather charts. The numbers in parentheses are frequencies at which measured arrival times were used to calculate distances. The lower of these two frequencies was used to estimate generation times.

Station	Distance calculated from measurements (km)	Distance (km) from weather charts based on: Storm center	Forward face of fetch
46002	2535 (0.04, 0.05)	3053	2017
46004	2239 (0.05, 0.06)	3071	2368
46005	1961 (0.04, 0.05)	2627	1591
46006	851 (0.03, 0.04)	1591	254
46022	2535 (0.04, 0.05)	3423	2054
46023	3090 (0.05, 0.06)	3256	1277
46024	2535 (0.04, 0.05)	3608	2240
46025	2239 (0.05, 0.06)	3552	1906

5. Other wave information and additional data interpretations

Another source of data for the storm of interest is wave data summarized by the Coastal Data Information Program (U.S. Army Corps of Engineers and State of California, 1983). Most of these measurements were made in shallow water with sensors on the bottom or mounted on piers and most of the measurement sites were partly sheltered from the storm waves by the coast or offshore islands. Long period wave energy generated by the storm would be considerably modified in these situations. However, two unsheltered Waverider buoys operated by the Coastal Data Information Program clearly show the investigated high wave height and long period event. A Waverider buoy in 320 m of water at 36°55.0′N, 122°19.5′W (off Monterey) measured long period swell with periods greater than 18 s arriving near 1013 GMT 10 February. This is consistent with arrival times at station 46022 to the north and at station 46023 to the south. Similarly, a Waverider buoy in 73 m of water at 37°56.3′N, 123°3.8′W (off Point Reyes) measured similar long period swell arriving between 0426 and 1027 GMT 10 February. This is also consistent with measurements at the data buoys. The 6 h interval between reported Waverider buoy measurements precludes precise determination of arrival times. The highest significant wave heights during the long period event were 5.16 and 5.29 m for the Monterey and Point Reyes Waverider buoys, respectively. These measurements also show that the studied event was the high wave height event associated with the longest periods during February 1983.

Wave data from the Coastal Data Information Program were used by Seymour (1983) to document the unusual severity of wave conditions along and off the California coast between January and March 1983. All of eight severe storms examined by Seymour (1983) had dominant wave periods between 17 and 22 s compared to only one storm which had a dominant wave period greater than 17 s in the previous three years. For those measurements made by Waverider buoys, low frequency roll-off associated

with the buoy electronics may have decreased low frequency wave energy and, for the nearshore measurements not made with buoys, shallow water effects would have modified the spectra at the long periods observed in 1983. The results provided by Seymour (1983) are of interest both for illustrating the unusual severity of wave conditions between January and March 1983, and for noting the occurrences of unusually long wave periods.

The U.S. Navy Fleet Numerical Oceanographic Center (FNOC) performs operational wave forecasts with a numerical directional wave spectra model. The primary features of this model are similar to those described by Pierson (1982). FNOC forecasts were obtained for model output locations in the vicinity of stations 46002, 46005, 46006 and 46022 off northern California. These locations were most directly affected by the high wave height and long period swell. Although wave energy at periods near 20 and 25 s was seen in the forecast spectra, the largest dominant wave periods were predicted to be 17.9 s, considerably shorter than the largest observed dominant wave periods of 25 s. Forecast swell arrival times at these long periods generally preceded actual swell arrival times. Under-estimation of dominant periods is consistent with low forecast wind speeds, and premature arrival times is consistent with storm winds closer to the stations than indicated by the measurements. Because of the steeply sloping low-frequency side of wind-generated wave spectra and the shift of the spectral peak toward lower frequencies as wind speeds increase, numerically modeled long-period wave energy is sensitive to wind speed. Differences between forecast and actual winds most likely account for the wave prediction discrepancies. These discrepancies indicate the potential importance of using measured wave data from the northern stations to improve forecasts of swell that would affect locations to the south.

Because an important application of wave data, particularly extreme wave data, is to validate wave models, a previously developed numerical directional wave spectra model (Earle *et al.*, 1982) was used to determine how well the model would work for the unusual measured wave conditions. Wind fields for the hindcast were prepared manually from 6-hour Northern Hemisphere surface weather charts by means of the geostrophic wind equation with simple corrections for atmospheric stability (e.g., U.S. Army Corps of Engineers, 1977) to provide winds at 19.5 m elevation, the wind input elevation to which the wave growth coefficients and spectral growth limitations in the model are keyed. Only local winds near each data buoy and winds associated with the two identified storms were input into the wave model. While winds could have been determined at all model grid points, separated by 120 n mi (222 km), a more efficient approach consistent with the supplemental use of the hindcast was to represent winds about the storms by between 10 and 16 rectangular fetches at each 6 h wind input time step. At each buoy station where measured winds were available, the speeds were adjusted to a 19.5 m elevation by means of a logarithmic profile, and the weather charts were used to define a local fetch. Hindcast directional wave spectra at the buoy locations were obtained by superposition of wave energy, propagated as swell from the storm regions, and locally-generated wind-wave energy. Swell energy was propagated from model grid points in the storm at frequency dependent group velocities along great circle routes in accordance with linear wave theory and previous observational studies (e.g., Snodgrass *et al.*, 1966) of swell propagation. The hindcast did not consider the storm as a point source in space or time.

Table 4 compares measured and hindcast peak energy arrival times for long periods corresponding to measured dominant periods. Figure 14 is an example of measured and hindcast significant wave height time histories. The hindcast time history is smoother than the measured time history because hindcast model input and output was at a 6 h interval compared to a 1 h measurement interval and because measured significant wave heights contain statistical sampling variability effects of ±10% to ±20% (e.g., Donelan and Pierson, 1983). The hindcast demonstrates that wave conditions at the buoy locations can be quantitatively related to storm meteorological con-

TABLE 4. Comparison of long period swell peak arrival times.

Station	Measured time (GMT)/date	Hindcast time (GMT)/date*	Time difference (h)
a. for 20 second waves			
46002	0700 February 10	0600 February 10	+1
46004	2100 February 9	0600 February 10	−9
46005	0600 February 10	0600 February 10	0
46006	1300 February 9	0000 February 10	−11
46022	1500 February 10	1800 February 10	−3
46023	1900 February 10	0000 February 11	−5
46024	0400 February 11	0600 February 11	−2
46025	0100 February 11	0000 February 11	+1
b. for 25 second waves			
46002	2200 February 9	0000 February 10	−2
46004	2000 February 9	0000 February 10	−4
46005	2300 February 9	0300 February 10	−4
46006	1300 February 9	1800 February 9	−5
46022	0600 February 10	0900 February 10	−3
46023	1700 February 10	1800 February 10	−1
46024	1900 February 10	0000 February 11	−5
46025	—	—	—

* Wave periods of 20 s and 25 s are between center periods of the hindcast model. Linear interpolation between hindcast time steps was used if different arrival times occurred adjacent to the periods of interest.

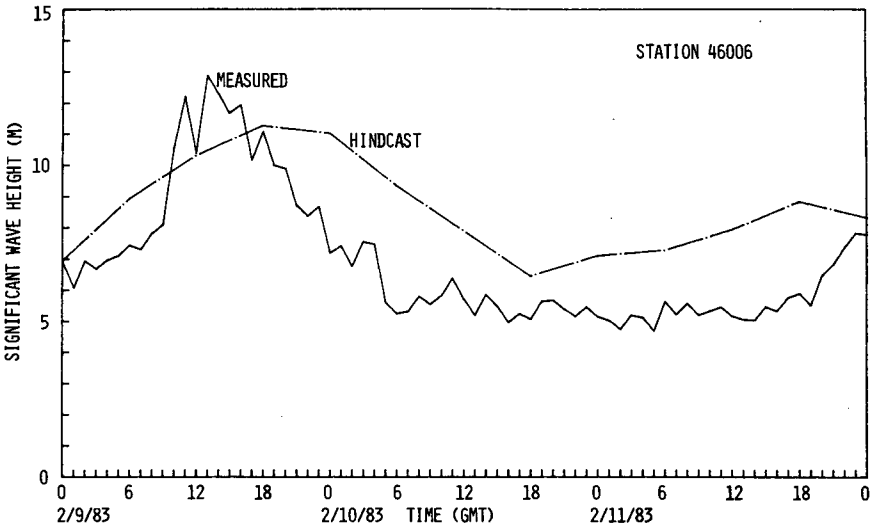

Fig. 14. Example of time histories of measured and hindcast significant wave height.

ditions. Hindcast arrival times in Table 4 are usually somewhat later than measured arrival times. Times of maximum significant wave heights at each buoy location also lagged measured times as seen in the example in Fig. 14. It is likely that the lack of good wind field data, which is a problem shared by nearly all wave modeling studies, is the cause of these discrepancies. For example, the noted behavior would occur if input wind speeds were not high enough or input fetches were not large enough. However, there are several other possibilities of importance for numerical wave modeling. There may be localized regions of strong gusty winds that are not depicted on weather charts but which could rapidly increase preexisting low-frequency energy. Based on wind variability investigations by Pierson (1983), wind speed variability of several m s^{-1} is possible and would increase the level of low frequency wave energy if included in the wave model input. Another possible factor is that the wave generation and dissipation mechanisms in the model, similar to those in the FNOC model and described by Pierson (1982), are based mainly on wave data when wind speeds were less than $\sim$20 m s^{-1}, while model input wind speeds in this storm ranged up to 32 m s^{-1}. Finally, swell propagation is based on linear wave theory whereas for the high measured and hindcast wave heights, propagation at a somewhat faster group velocity corresponding to nonlinear waves could be appropriate.

6. Summary and conclusions

The described long period wave event was very unusual in that high waves with exceptionally long periods of 20–25 s were measured by the data buoys off the west coast of the United States. These waves were primarily generated between 0000 GMT 8 February and 1200 GMT 9 February during a severe storm in the northeast Pacific Ocean. Large wave generation fetches on the order of 1000 km with high speeds often around 30 m s^{-1} south of the storm center contributed to generation of high long-period waves that propagated toward the west coast. These waves arrived at various buoys between 9 and 11 February depending on the distance of each buoy from the wave generation regions. Propagation of the long period waves as swell was consistent with classical concepts of energy propagation at group velocities along great circle routes. At all buoys, wave conditions at the time of highest wave heights had substantial swell contributions.

General comparisons of the measurement results to FNOC wave forecasts and a wave hindcast have implications for wave model development and validation. Of most importance is the sensitivity of long-period swell arrival times and heights to wind speed probably because of the steeply sloping low-frequency side of wind-generated wave spectra. Small changes in wind speed can substantially change energy levels of low-frequency wave energy. Model output accuracy may also be affected by poor portrayal of local regions of high gusty winds on weather charts and by use of theory mainly developed from use of wave data at lower wind speeds. When wave predictions are made, forecast winds, that cannot be perfectly accurate, must be used so that additional errors for long period swell heights and arrival times may occur. Thus, the ability to identify high swell at northern buoys prior to its arrival at southern buoys may have real-time forecast applications. For example, if swell that is not predicted at the northern buoys is detected at these buoys, it would be possible to determine the likely wave generation region and to repeat the forecast

using the northern buoy wave data as calibration data to adjust input wind fields, thus improving forecast accuracies off southern California. An efficient wave prediction model could also be developed to generate waves in the vicinity of storms and propagate wave energy to coastal sites. Such a model could operate on small computers to facilitate use by forecasters. Improvements for swell prediction are important because southern California is vulnerable to high swell from storms in the northeast Pacific Ocean. As noted by Seymour (1983) and the NOAA publication *Storm Data* (NOAA, 1983), high waves that occurred during early 1983 caused major damage along the California coast. Such damage is not unique to the severe storms that occurred in 1983. As an example, Shields (1970) describes extensive damage at Redondo Beach near Los Angeles caused by high swell (4–6 m breaker heights) from a major storm in the Gulf of Alaska in December 1969.

Consideration of data buoy wave measurements to increase wave prediction accuracy indicates a potential limitation with the present data buoy network. Many of the southern buoys, including several in shallow water which were not used for this study, are partly sheltered from incoming swell either by part of the coastline or islands. These buoys are also too close to many vulnerable sections of coastline to provide sufficient advance warnings of high swell. A southernmost data buoy farther offshore would be useful for prediction of swell both from storms in the North Pacific Ocean as well as storms in the South Pacific. Capability of Southern Hemisphere storms to generate long period swell that can be substantially amplified in shallow water along the California coast has been documented (e.g., Horrer, 1950).

A final conclusion is that the wave-data base from the data buoys during the investigated high-wave height and long-period event and other high-wave events during January through March 1983 represents an important resource which should be further utilized for projects, such as studies of wave generation theories and development of improved numerical wave models. In addition to the wave measurements at the eight data buoys used for this study, the long-period swell event was monitored by other data buoys in relatively shallow water. Wave data mainly at shallow locations are also available from more than a dozen locations instrumented by the Coastal Data Information Program. The data closer to shore that were not used for this project should be valuable for investigation of shallow water wave effects and development of shallow-water wave models.

Acknowledgments. The authors thank personnel of the NOAA Data Buoy Center for their efficient preparation of various data analysis products. Dr. Joseph M. Bishop worked with the authors in preparing storm wind fields for use with the wave hindcast model. Dr. Larry Hsu provided useful information and participated in several discussions during this work. Dr. Richard J. Seymour provided valuable information about wave measurements made by the Coastal Data Information Program. Mr. Elwyn E. Wilson of the *Mariners Weather Log* was helpful in providing NMC ship reports. The staff of the NOAA National Environmental Satellite, Data, and Information Service helped locate the satellite images. The work reported here was supported by the NOAA Data Buoy Center under Computer Sciences Corporation subcontract to Marine Environments Corporation.

REFERENCES

Donelan, M., and W. J. Pierson, 1983: The sampling variability of estimates of spectra of wind-generated gravity waves. *J. Geophys. Res.*, **88**, 4381–4392.

Earle, M. D., and K. A. Bush, 1982: Strapped-down accelerometer effects on NDBO wave measurements. *Proc. Oceans '82*, Washington, DC, Mar. Technol. Soc. and IEEE, 838–848.

——, ——, J. M. Bishop and E. E. Lacour, 1982: Development of a global ocean swell model. *Offshore Technol. Conf.*, Houston, 329–337.

Horrer, P. L., 1950: Southern Hemisphere swell and waves from a tropical storm at Long Beach, California. U.S. Army Corps of Engineers Beach Erosion Board Bull., 4.

Longuet-Higgins, M. S., 1980: On the distribution of the heights of sea waves: Some effects of nonlinearity and finite band width. *J. Geophys. Res.*, **85**, 1519–1523.

NOAA (National Oceanic and Atmospheric Administration), 1983: *Storm Data.* February, 1983, **25**, 11.

NOAA Data Buoy Center, 1983: *Climatic Summaries for NOAA Data Buoys.* NOAA, 214 pp.

Parsons, C. L., 1979: On the remote detection of swell by satellite radar altimeter. *Mon. Wea. Rev.*, **107**, 1210–1218.

Pierson, W. J., 1982: The spectral ocean wave model (SOWM), a Northern Hemisphere computer model for specifying and forecasting ocean wave spectra. David W. Taylor Naval Ship Research and Development Center, Rep. DTNSRDC-82/011.

——, 1983: The measurement of the synoptic scale wind over the ocean. *J. Geophys. Res.*, **88**, 1683–1708.

Seymour, R. J., 1983: Extreme waves in California during winter, 1983. State of California, the Resources Agency, Department of Boating and Waterways, 17 pp.

Shields, G. C., 1970: Sea state and surf forecasting in southern California. *Mar. Wea. Log*, **14**, 257–259.

Snodgrass, F. E., G. W. Groves, K. F. Hasselmann, G. R. Miller, W. H. Munk and W. H. Powers, 1966: Propagation of ocean swell across the Pacific. *Phil. Trans. Roy. Soc. London*, **A295**, 431–497.

Steele, K. E., and M. D. Earle, 1979: The status of data produced by NDBO Wave Data Analyzer (WDA) systems. *Proc. Oceans '79*, San Diego, Mar. Technol. Soc. and IEEE, 212–220.

Sverdrup, H. U., and W. H. Munk, 1947: *Wind Sea and Swell: Theory of Relations for Forecasting.* H.O. Publication 601, U.S. Navy Oceanographic Office.

U.S. Army Corps of Engineers, 1977: *Shore Protection Manual*, 3rd ed., Vol. 1, 514 pp.

——, and State of California, the Resources Agency, Department of Boating and Waterways, 1983: Coastal Data Information Program, Monthly Rep. February 1983, Monthly Summary Rep. No. 87.